chemosensors

*Communication*

# A GSH-Activatable Theranostic Prodrug Based on Photoinduced Electron Transfer for Cancer Fluorescence Imaging and Therapy

**Xuan Zhao [1], Xiaolong Zeng [2,*], Xinyu Wu [3], Lihong Shi [1], Sumin Zhu [1,*] and Wen Sun [2,*]**

[1] Digestive Medicine Center, The Second Affiliated Hospital of Xuzhou Medical University, Xuzhou 221000, China; xyefyzhaoxuan@163.com (X.Z.); slh0186@126.com (L.S.)
[2] State Key Laboratory of Fine Chemicals, Dalian University of Technology, Dalian 116024, China
[3] The Second Affiliated Hospital of Nanjing Medical University, Nanjing 211103, China; wuxinyu642@gmail.com
* Correspondence: zeng123@dlut.edu.cn (X.Z.); njzhusumin@163.com (S.Z.); sunwen@dlut.edu.cn (W.S.)

**Abstract:** Traditional chemotherapeutic drugs have limitations due to their non-targeted ability toward cancer cells. Stimuli-activatable prodrugs are designed to overcome these obstacles. However, the real-time monitoring of stimuli-activatable theranostic prodrugs still poses challenges. Herein, a prodrug (Fe–SS–HCy), consisting of a ferrocene-modified hemicyanine linked via a disulfide bond, is synthesized for anticancer imaging and therapy. Before activation, the toxicity of Fe–SS–HCy is low. The fluorescence of Fe–SS–HCy is quenched by ferrocene due to photoinduced electron transfer. After being taken up by cancer cells, the intracellular GSH activates Fe–SS–HCy, which releases HCy. The fluorescence of HCy is restored and selectively accumulates in the mitochondria, which further produce reactive oxygen species (ROS) to induce cancer cell death. Thus, this "off-on" fluorogenic HCy presents a new strategy for monitoring prodrug activation in real-time and for enhancing therapeutic efficacy with reduced side effects.

**Keywords:** fluorescent dye; cancer imaging; activatable prodrug; photoinduced electron transfer; cancer therapy; hemicyanine

check for updates

**Citation:** Zhao, X.; Zeng, X.; Wu, X.; Shi, L.; Zhu, S.; Sun, W. A GSH-Activatable Theranostic Prodrug Based on Photoinduced Electron Transfer for Cancer Fluorescence Imaging and Therapy. *Chemosensors* **2023**, *11*, 397. https://doi.org/10.3390/chemosensors11070397

Academic Editor: Andrea Pucci

Received: 31 May 2023
Revised: 6 July 2023
Accepted: 12 July 2023
Published: 15 July 2023



## 1. Introduction

Among various cancer treatments, chemotherapy is the dominant method, which relies mainly on cytotoxic drugs to inhibit cancer cell growth [1]. However, it still poses challenges in the clinic. Traditional chemotherapeutic drugs lack selectivity between cancer cells and normal cells [2], causing severe side effects by damaging healthy cells [3]. Additionally, reduced dosages of anticancer drugs at tumor sites may limit their efficacy and potentially lead to drug resistance [4]. To overcome these challenges, stimuli-activatable prodrugs have shown significant progress in recent years [5]. These prodrugs exhibit no toxicity in noncancerous tissues and can be specifically activated at tumor sites [6]. Once activated by a specific tumor-associated factor, their toxicity can be efficiently enhanced [7]. The tumor-specific activation of prodrugs has shown improved selectivity and reduced side effects, as the specific tumor microenvironment exclusively activates the prodrugs at tumor tissues and is non-toxic toward normal tissues [8,9].

The unique metabolic environment of tumors, such as acidic conditions [10], excessive expression of reactive oxygen species (ROS) [11], and overexpression of enzymes [12], can be exploited as triggers for the activation of prodrugs. Moreover, cancer cells have significantly higher concentrations of glutathione (GSH) than normal cells, making the GSH-activatable strategy promising [13]. GSH is a highly abundant biothiol in living cells, which plays a pivotal role in physiological processes such as redox homeostasis and cellular growth [14]. GSH-activatable prodrugs can be designed to be stable during

blood circulation but become selectively activated by GSH within cancer cells, leading to enhanced drug efficacy and reduced systemic toxicity. Furthermore, the high sensitivity and rapid response of GSH-activatable prodrugs allow for precise drug release at the tumor site [15].

Regarding activatable prodrugs, the real-time tracking of drug release is of great interest [16]. A commonly used method for monitoring drug release is to design theranostic prodrugs through the conjugation of fluorescent dyes with therapeutic drugs [17,18]. However, most of the fluorescence of theranostic prodrugs is always in the turn-on state, which is constrained by factors such as photobleaching, variations in assay conditions, and inadequate sensitivity for accurate detection [19]. Therefore, it is crucial to develop prodrugs with a unique fluorescence "off-on" property that serves as a switch to turn on the fluorescence for tracking drug release.

Herein, the design of a GSH-activatable theranostic prodrug Fe–SS–HCy is reported. Fe–SS–HCy consists of a GSH-cleavable disulfide bond, a ferrocene moiety, and fluorescent hemicyanine (HCy) for imaging and therapeutic effects (Figure 1). Ferrocene is recognized as a potent quencher due to its ability to donate electrons, which can quench the fluorescence of organic fluorophores through a photoinduced electron transfer (PET) process [20]. HCy has a good therapeutic effect with strong red fluorescence, making it an ideal theranostic anticancer drug [17,21]. Before activation, the fluorescence of Fe–SS–HCy is in the off state due to the PET process by ferrocene. Moreover, the cytotoxicity of Fe–SS–HCy is low. After the internalization by cancer cells, the overexpressed intracellular GSH cleaves the disulfide bond in Fe–SS–HCy and releases HCy species. The released HCy selectively accumulates in the mitochondria, generating ROS to kill cancer cells. Meanwhile, HCy exhibits strong fluorescence, making it suitable for monitoring drug release in real-time. The GSH activation of Fe–SS–HCy only occurs in cancer cells, which further improves the selectivity for tumor tissues. Fe–SS–HCy exhibits GSH-enhanced cytotoxicity and drug release monitoring, enabling effective theranostic effects for cancer therapy.

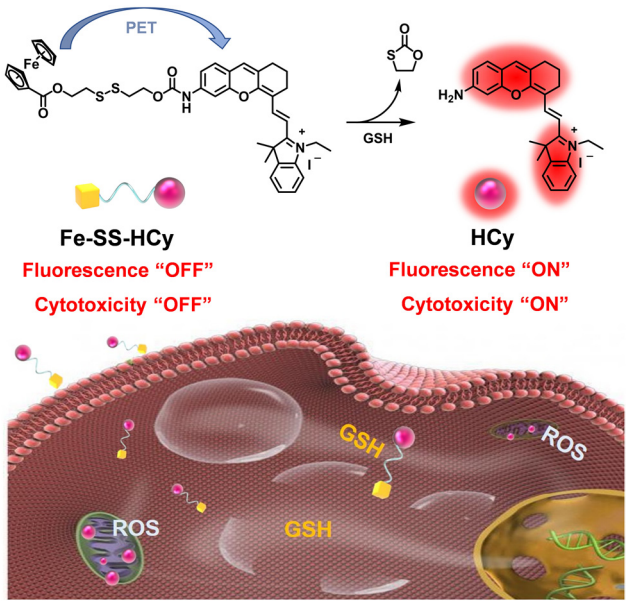


**Figure 1.** Chemical structure of Fe–SS–HCy and GSH activation of fluorescence and cytotoxicity process in cancer cells.

## 2. Materials and Methods

2,3,3-Trimethylindolenine (98%), iodoethane (99%), phosphorus oxychloride (99%), cyclohexanone (99%), 3-Nitrophenol (99%), $SnCl_2$ (98%), ferrocenecarboxylic acid (97%), and 4-dimethylaminopyridine (DMAP) were purchased from Aladdin Ltd, Shanghai, China. 2,2′-dithiodiethanol (90%), *N*,*N*′-dicyclohexylcarbodiimide (DCC) (99%), and *p*-nitrophenyl

chloroformate (98%) were purchased from J&K Scientific Ltd, Beijing, China. All other solvents were of analytic grade. Milli-Q water with a resistivity of 18.2 MΩ·cm was used in this study. All reactions were monitored via thin layer chromatography (TLC) using 0.25 mm silica gel plates with a UV indicator (GF-254).

$^1$H nuclear magnetic resonance ($^1$H NMR) was recorded using a 400-MHz Bruker Spectrospin NMR spectrometer at 25 °C. High resolution mass spectrometric (HRMS) data were obtained using an LTQ Orbit rap XL instrument. UV–vis absorption spectra were measured on a Lambda 900 spectrometer (Perkin Elmer, Waltham, MA, USA). Fluorescence spectra were recorded on a TIDAS II spectrometer (J&M, Essingen, Germany).

The energies of the optimized geometries of all compounds were determined by using the density functional theory (DFT) method with the Becke, three-parameter, Lee–Yang–Parr (B3LYP) hybrid functional for exchange correlation and LanL2DZ in the form of a basis set. The optimized geometries of all compounds are shown in Figure S15. The calculations were performed using the Gaussian 09W and GaussView 5.0.8 software.

## 3. Results

The synthesis of Fe–SS–HCy is depicted in ESI† (Figures S1 and S2). Trimethylindolenine was used as the starting compound, which reacted with iodoethane via an N alkylation reaction. This intermediate 1 underwent a condensation reaction with compound **2** [22], followed by the decoration of the CyCl intermediate with 3-nitrophenol, nitro reduction, and cyclization to produce HCy. Fe–SS–OH was synthesized through condensation between 2,2′-dithiodiethanol and ferrocene derivate. The hydroxyl group of Fe–SS–OH was further activated with *p*-nitrophenyl chloroformate (NPC), and conjugated with the amine group of HCy to give Fe–SS–HCy in a moderate yield (82%). Fe–SS–HCy and each intermediate were characterized by nuclear magnetic resonance (NMR) spectroscopy and high-resolution mass spectrometry (HRMS) (Figures S3–S14).

We studied the absorption response of Fe–SS–HCy toward GSH using UV–vis spectroscopy (Figure 2a). Fe–SS–HCy exhibited a broad absorption band from ≈400 to ≈850 nm, in which the maximum peak was located at ≈690 nm. After incubation with GSH, the maximum peak blue-shifted to 670 nm. This spectral change was consistent with the maximum absorption of HCy, indicating that GSH was able to cleave the disulfide bond and release HCy (Figure 2b). The released HCy was fluorescent. Thus, the fluorescence response of Fe–SS–HCy toward GSH was further investigated. The laser excitation wavelength was set at 610 nm and the emission range from 650 to 850 nm with a scan speed of 1 nm/s. The photostability of Fe–SS–HCy caused by red-light irradiation was then excluded (Figure S15). Subsequently, in the absence of GSH, a weak fluorescence peak at ≈710 nm was observed in the fluorescence spectrum of Fe–SS–HCy. After incubation with 1 mM GSH for 30 min, the fluorescence intensity at 710 nm slightly increased. When increasing the GSH concentration from 1 mM to 10 mM, the fluorescence intensity significantly intensified as a function of GSH concentration (Figure 2c). Furthermore, we examined the fluorescence response of Fe–SS–HCy over time in the presence of 5 mM GSH. The fluorescence peak was slightly red-shifted to 730 nm and its intensity increased up to 20-fold as a function of incubation time (Figure 2d). The increased fluorescence intensities and response time toward GSH were comparable to the previous studies [17,23]. We infer that the increase in fluorescence intensity is attributed to the released fluorescent HCy, the fluorescence of which was quenched by the ferrocene unit in Fe–SS–HCy before incubation with GSH.

The quenching mechanism can be rationalized by investigating the energy level difference between the lowest unoccupied molecular orbital (LUMO) and highest occupied molecular orbital (HOMO) of ferrocene and HCy (Figures 3 and S16). The density functional theory (DFT) calculations revealed that the LUMO energy of ferrocene is located between the LUMO and HOMO energies of HCy. Therefore, electron transfer occurred from the excited state of HCy to the LUMO of ferrocene, resulting in fluorescence quenching. However, upon the addition of GSH, the thiol group cleaved the disulfide bond in

Fe–SS–HCy, leading to the release of the fluorescent HCy species. We also analyzed the cleaved products using HRMS measurement (Figure S17) and found an obvious peak at $m/z$ 290.0757, corresponding to the Fe-SH species. This observation indicates that GSH can successfully cleave the disulfide bond in Fe–SS–HCy, forming Fe–SH species and HCy species, which enhances the fluorescence.

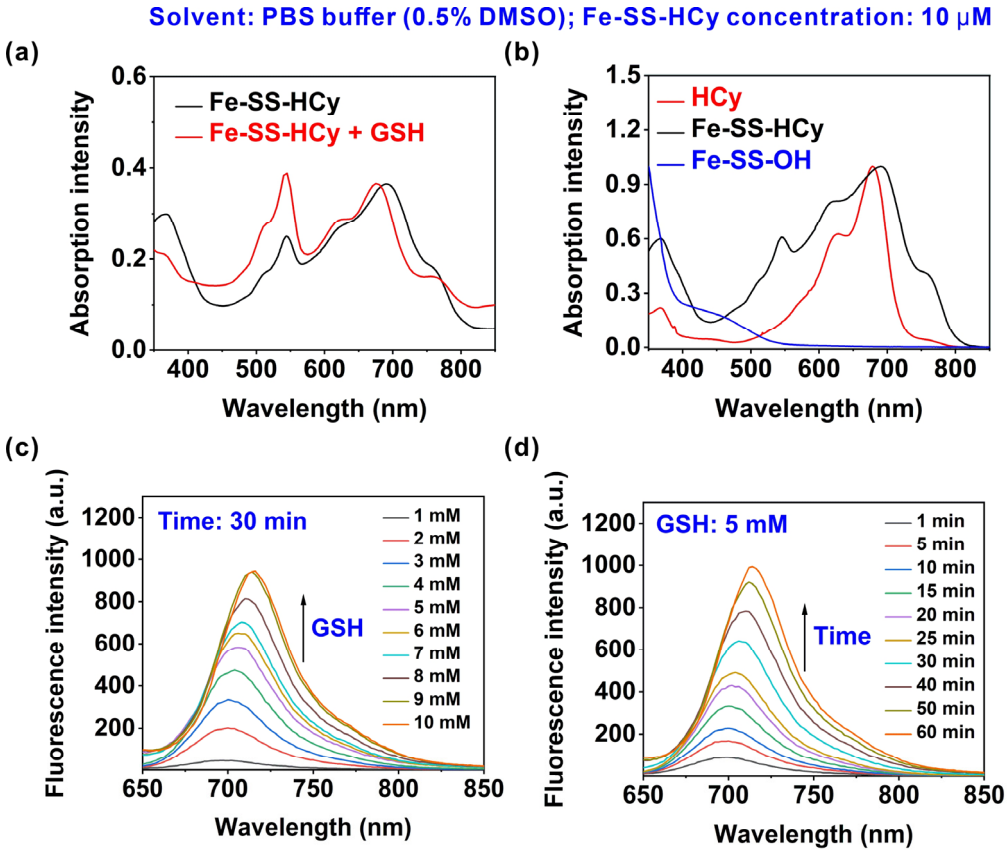


**Figure 2.** (**a**) Normalized absorption intensities of Fe–SS–HCy before and after GSH treatment. (**b**) Normalized absorption intensities of HCy, Fe–SS–HCy, and Fe-SS-OH. (**c**) Fluorescence spectra of Fe–SS–HCy treated with GSH at different concentrations. (**d**) Fluorescence spectra of Fe–SS–HCy treated with GSH for different times.

Given that GSH is overexpressed in cancer cells [24], we further investigated the potency of Fe–SS–HCy in response to GSH in MCF-7 cells. The intracellular cleavage of Fe–SS–HCy was imaged using confocal laser scanning microscopy (CLSM) to detect the fluorescence of the released HCy (Figure 4a). Initially, Fe–SS–HCy was weakly fluorescent because the fluorescence of HCy was quenched by the ferrocene unit. However, after incubating it with MCF-7 cells for 60 min, red fluorescence signals were observed, suggesting that Fe–SS–HCy was taken up by cells and the intracellular GSH activated the fluorescent HCy. The red fluorescence became brighter and stronger after 120 min and 180 min of incubation. The time-dependent increase in intracellular fluorescence was also quantified using the fluorescence intensities of CLSM (Figure S18). The intracellular fluorescence intensity was ≈42% after an incubation time of 60 min, which was gradually increased up to ≈60% over time to up to 180 min. These results indicate that the intracellular GSH cleaved the disulfide bond of Fe–SS–HCy and activated the fluorescence signals of HCy over time.

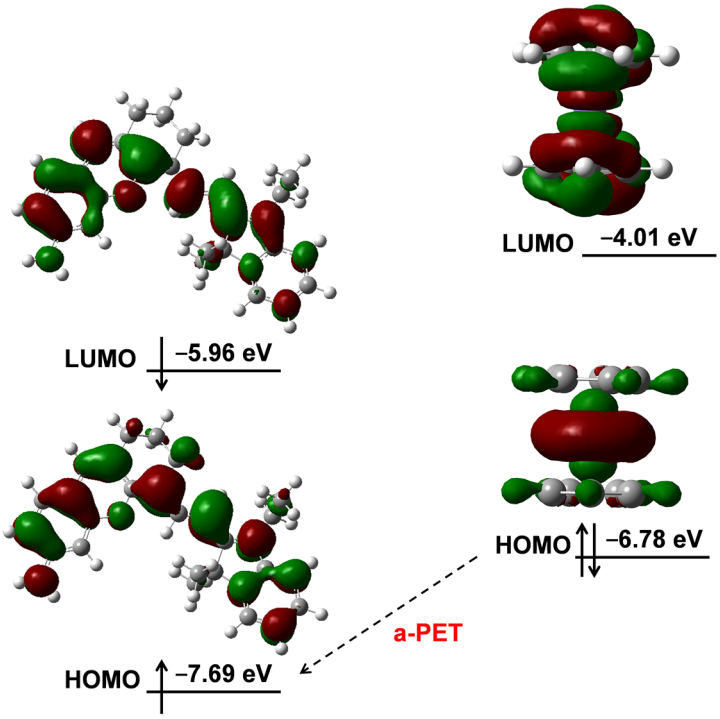


**Figure 3.** Frontier molecular orbital energy illustration of HCy and ferrocene is used to elaborate on PET mechanism. a-PET refers to the process in which electron transfer from the receptor to the fluorophore.

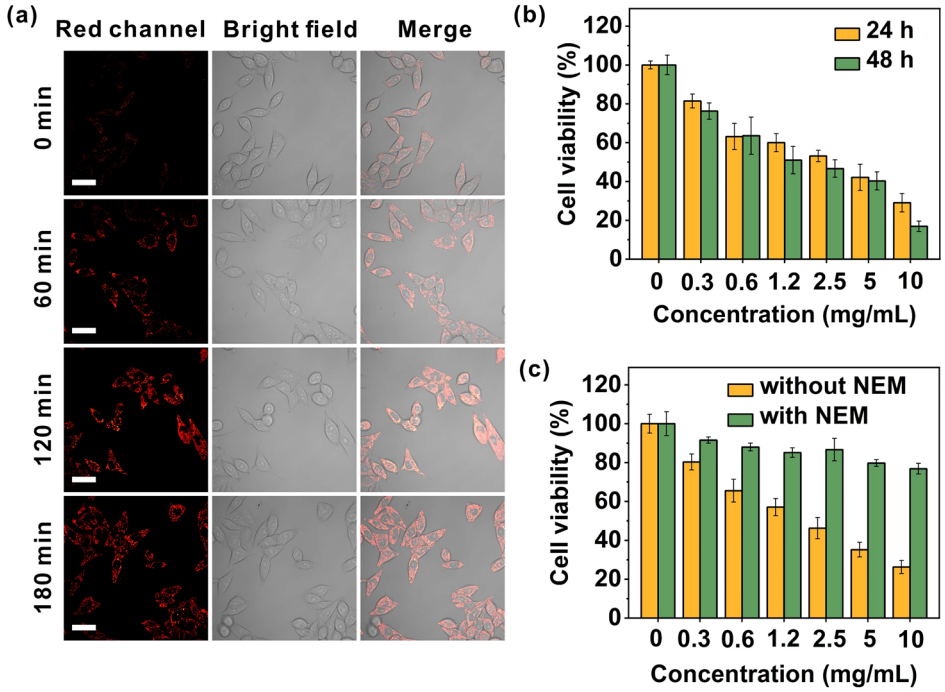


**Figure 4.** (**a**) Confocal laser scanning microscopy (CLSM) images of Fe–SS–HCy (red) after incubation with MCF-7 cancer cells for different time periods. Scale bars: 50 μm. (**b**) Cell viability of MCF-7 cells treated with different concentrations of Fe–SS–HCy with the incubation time of 24 h or 48 h. (**c**) Cell viability of MCF-7 cells treated with different concentrations of Fe–SS–HCy in the presence or absence of NEM pretreatment.

HCy is an anticancer agent and can inhibit the growth of cancer cells [17,21]. We studied the anticancer performance of Fe–SS–HCy, which can produce HCy under intracellular reduction environments (Figure 4b). After incubation with 0.3 mg/mL Fe–SS–HCy for 24 h and 48 h, the cell viability slightly decreased to ≈82% and ≈77%, respectively. However, when the concentration of Fe–SS–Hcy was increased to 2.5 mg/mL, nearly half of the cancer cells were killed. As the concentration of Fe–SS–HCy further increased, the cell viabilities continued to decrease. When the concentration of Fe–SS–HCy reached 10 mg/mL, the cell viabilities decreased to ≈31% and ≈18% after 24 h and 48 h of incubation, respectively. We infer that the decrease in cell viability was due to the production of HCy via the cleavage of the disulfide bond in Fe–SS–HCy. A higher concentration of Fe–SS–HCy and a longer incubation time generated more HCy, thereby enhancing the cytotoxicity towards cancer cells.

We concluded that the inhibition of MCF-7 cell growth via Fe–SS–HCy was due to the production of HCy. Cytotoxicity under different intracellular GSH concentration was further studied. N-Ethylmaleimide (NEM) was applied to control the intracellular GSH concentration because NEM is a biothiol scavenger, which can reduce the biothiol concentration in living cells [25]. We investigated cell viability in the presence or absence of NEM (Figure 4c). Fe–SS–HCy showed enhanced cytotoxicity as the concentration gradually increased from 0.3 mg/mL to 10 mg/mL. However, when the cancer cells were pretreated with NEM, the incubation of cancer cells with Fe–SS–HCy did not significantly decrease the cell viability. Even when the concentration of Fe–SS–HCy reached 10 mg/mL, cell viability decreased by less than 20%. The intracellular cleavage of Fe–SS–HCy under different intracellular GSH concentrations was also imaged (Figure S19). Fe–SS–HCy incubated with MCF-7 cells showed strong red fluorescence. As a contrast, negligible fluorescence was detected in the cancer cells in the presence of NEM. However, the fluorescence was switched on upon the further addition of GSH. These results demonstrate that the red fluorescence signal was attributed to the produced HCy, which was caused by intracellular GSH and led to cancer cell death.

To verify the subcellular localization of HCy, we stained the lysosomes, nucleus, mitochondria, and lipid droplets in MCF-7 cells using LysoTracker, Hoechst 33342, MitoTracker, and Nile Red, respectively. We compared their fluorescence with that of HCy (red fluorescence) (Figure 5). HCy overlapped well with MitoTracker (green fluorescence), and the Pearson correlation coefficient between them was calculated to be 0.93. However, the Pearson correlation coefficients between HCy and LysoTracker, Hoechst 33342, and Nile Red were 0.61, 0.03, and 0.43, respectively. These results demonstrated that HCy was selectively localized in the mitochondria, where it accumulated and led to mitochondrial membrane damage. The destruction of the mitochondrial structure and function may decrease the oxygen consumption rate and mitochondrial respiration rate, affecting the intracellular reactive oxygen species (ROS) level [26]. Thus, we used 2′,7′-dichlorofluorescin diacetate (DCFH-DA) to detect the intracellular ROS level after Fe–SS–HCy treatment (Figure S20). Negligible fluorescence was observed in the control group or in the MCF-7 cells treated with the DCFH-DA probe only or Fe–SS–HCy only. These observations indicated that no ROS was generated under these conditions. However, strong fluorescence was detected when MCF-7 cells were treated with Fe–SS–HCy, followed by probe incubation. These results demonstrated high ROS generation, which caused cytotoxicity towards MCF-7 cells.

Regarding the higher GSH concentration in cancer cells, Fe–SS–HCy exhibited a specific imaging of cancer cells compared to normal cells. The intracellular fluorescence activation of Fe–SS–HCy in different kinds of cancer cells and normal cells was studied using CLSM (Figure S21). When Fe–SS–HCy was incubated with the MCF-7, A549, and BEL-7404 cells, red fluorescence was observed in these cancer cell lines. However, negligible fluorescence was detected when it was incubated with human umbilical vein endothelial (HUVEC) normal cells. The intracellular fluorescence intensities of cancer cells were quantified to be three times higher than that of normal cells (Figure S22), suggesting that Fe–SS–HCy can specifically image cancer cells.

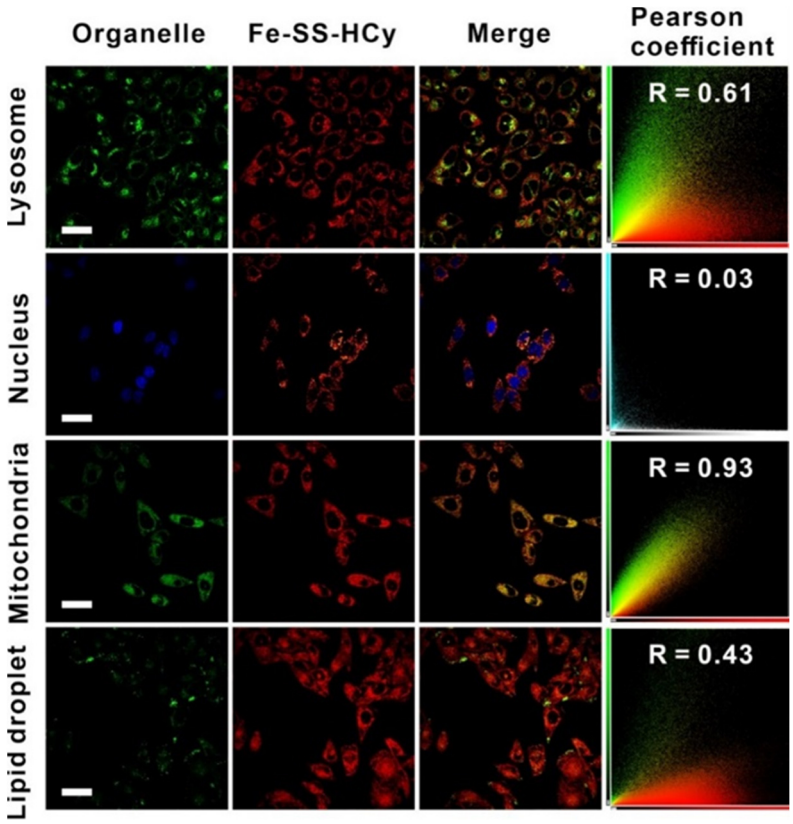


**Figure 5.** Colocalization with lysosome in MCF-7 cancer cells and Pearson coefficients (R) of released HCy. HCy was excited with a 635 nm laser (shown in red). Lysosome was labeled using LysoTracker Red, which was excited with a 561 nm laser (shown in green). Nucleus was labeled using Hoechst 33342, which was excited with a 405 nm laser (shown in blue). Mitochondria were labeled using MitoTracker Red, which was excited with a 561 nm laser (shown in green). Lipid droplet was labeled using Nile Red, which was excited with a 561 nm laser (shown in green). The lysosome, mitochondria, and lipid droplet are shown in false colors to better distinguish them from those of HCy. Scale bars: 50 μm.

## 4. Conclusions

In conclusion, we designed a ferrocene-modified hemicyanine, Fe–SS–HCy, for application in cancer treatment. The fluorescence and cytotoxicity of Fe–SS–HCy are blocked due to the PET mechanism. Fe–SS–HCy exhibited GSH-activatable cytotoxicity and fluorescence because GSH cleaved the disulfide bond and released HCy. The fluorescent HCy accumulated in the mitochondria, inducing ROS generation to inhibit cancer cell growth. Our study identified a new strategy for PET-based prodrugs. We believe that more theranostic prodrugs could be developed using stimuli-enhanced cytotoxicity and fluorescence for cancer therapy.

**Supplementary Materials:** The following supporting information can be downloaded at https://www.mdpi.com/article/10.3390/chemosensors11070397/s1, Figure S1: synthetic route of HCy; Figure S2: synthetic route of Fe–SS–HCy; Figure S3: $^{1}$H NMR of compound **2**; Figure S4: $^{1}$H NMR of CyCl; Figure S5: $^{1}$H NMR of compound **3**; Figure S6: HRMS of compound **3**; Figure S7: $^{1}$H NMR of HCy; Figure S8: HRMS of compound HCy; Figure S9: $^{1}$H NMR of Fe–SS–OH; Figure S10: HRMS of compound Fe-SS-OH; Figure S11: $^{1}$H NMR of Fe–SS–NPC; Figure S12: HRMS of compound Fe–SS–NPC; Figure S13: $^{1}$H NMR of Fe–SS–HCy; Figure S14: HRMS of compound Fe–SS–HCy; Figure S15: stability of Fe–SS–HCy upon light irradiation; Figure S16: optimized structures of HCy and ferrocene calculated by density functional theory (DFT); Figure S17: The HRMS spectra of Fe–SS–HCy after GSH treatment; Figure S18: Intracellular fluorescence of MCF-7 cells after incubation with Fe–SS–HCy for different time period; Figure S19: CLSM images of MCF-7 cancer cells treated with only Fe–SS–

HCy, Fe–SS–HCy + NME and Fe–SS–HCy + NEM + GSH; Figure S20: generation of intracellular ROS in MCF-7 cells as observed by CLSM; Figure S21: fluorescence imaging of endogenous GSH for cancer cell recognition; Figure S22: the relative fluorescence intensities between different cells.

**Author Contributions:** Conceptualization, X.Z. (Xuan Zhao), X.Z. (Xiaolong Zeng), S.Z. and W.S.; methodology, X.Z. (Xuan Zhao), X.Z. (Xiaolong Zeng), X.W. and L.S.; software, X.Z. (Xuan Zhao), X.Z. (Xiaolong Zeng), X.W. and L.S.; validation, X.Z. (Xuan Zhao), X.Z. (Xiaolong Zeng), X.W., L.S., S.Z. and W.S.; formal analysis, X.Z. (Xuan Zhao), X.Z. (Xiaolong Zeng), X.W., L.S., S.Z. and W.S.; investigation, X.Z. (Xuan Zhao), X.Z. (Xiaolong Zeng); resources, L.S., S.Z. and W.S.; data curation, X.Z. (Xuan Zhao) L.S., S.Z. and W.S.; writing—original draft preparation, X.Z. (Xuan Zhao), X.W. and L.S.; writing—review and editing, X.Z. (Xuan Zhao), X.Z. (Xiaolong Zeng), X.W., L.S., S.Z. and W.S.; visualization, X.Z., S.Z. and W.S.; supervision, X.Z. (Xiaolong Zeng), S.Z. and W.S.; project administration, X.Z., S.Z. and W.S.; funding acquisition, X.Z., S.Z. and W.S. All authors have read and agreed to the published version of the manuscript.

**Funding:** This work was financially supported by the National Natural Science Foundation of China (22208046, 22078046), the China Postdoctoral Science Foundation (2023M730470), the Development Fund of the Affiliated Hospital of Xuzhou Medical University (XYFY2020044), and Xuzhou Key R&D Plan (Social Development) (KC22210).

**Institutional Review Board Statement:** Not applicable.

**Informed Consent Statement:** Not applicable.

**Data Availability Statement:** Not applicable.

**Conflicts of Interest:** The authors declare no conflict of interest.

## References

1. Johnstone, T.C.; Suntharalingam, K.; Lippard, S.J. The Next Generation of Platinum Drugs: Targeted Pt(II) Agents, Nanoparticle Delivery, Pt(IV) Prodrugs. *Chem. Rev.* **2016**, *116*, 3436–3486. [CrossRef] [PubMed]
2. Bhatt, A.P.; Pellock, S.J.; Biernat, K.A.; Walton, W.G.; Wallace, B.D.; Creekmore, B.C.; Letertre, M.M.; Swann, J.R.; Wilson, I.D.; Roques, J.R. Targeted Inhibition of Gut Bacterial β-Glucuronidase Activity Enhances Anticancer Drug Efficacy. *Proc. Natl. Acad. Sci. USA* **2020**, *117*, 7374–7381. [CrossRef]
3. Wang, Q.; Dai, Y.; Xu, J.; Cai, J.; Niu, X.; Zhang, L.; Chen, R.; Shen, Q.; Huang, W.; Fan, Q. All-in-One Phototheranostics: Single Laser Triggers NIR-II Fluorescence/Photoacoustic Imaging Guided Photothermal/Photodynamic/Chemo Combination Therapy. *Adv. Funct. Mater.* **2019**, *29*, 1901480. [CrossRef]
4. Lin, G.; Mi, P.; Chu, C.; Zhang, J.; Liu, G. Inorganic Nanocarriers Overcoming Multidrug Resistance for Cancer Theranostics. *Adv. Sci.* **2016**, *3*, 1600134. [CrossRef] [PubMed]
5. Seidi, F.; Zhong, Y.; Xiao, H.; Jin, Y.; Crespy, D. Degradable Polyprodrugs: Design and Therapeutic Efficiency. *Chem. Soc. Rev.* **2022**, *51*, 6652–6703. [CrossRef]
6. Zhou, F.; Feng, B.; Yu, H.; Wang, D.; Wang, T.; Ma, Y.; Wang, S.; Li, Y. Tumor Microenvironment-Activatable Prodrug Vesicles for Nanoenabled Cancer Chemoimmunotherapy Combining Immunogenic Cell Death Induction and CD47 Blockade. *Adv. Mater.* **2019**, *31*, 1805888. [CrossRef]
7. Dutta, D.; Zhou, Q.; Mukerabigwi, J.F.; Lu, N.; Ge, Z. Hypoxia-Responsive Polyprodrug Nanocarriers for Near-Infrared Light-Boosted Photodynamic Chemotherapy. *Biomacromolecules* **2021**, *22*, 4857–4870. [CrossRef]
8. Li, S.-Y.; Liu, L.-H.; Jia, H.-Z.; Qiu, W.-X.; Rong, L.; Cheng, H.; Zhang, X.-Z. A pH-Responsive Prodrug for Real-Time Drug Release Monitoring and Targeted Cancer Therapy. *Chem. Commun.* **2014**, *50*, 11852–11855. [CrossRef]
9. Liang, H.; Zhou, Z.; Luo, R.; Sang, M.; Liu, B.; Sun, M.; Qu, W.; Feng, F.; Liu, W. Tumor-Specific Activated Photodynamic Therapy with An Oxidation-Regulated Strategy for Enhancing Anti-Tumor Efficacy. *Theranostics* **2018**, *8*, 5059. [CrossRef]
10. Migliorini, F.; Cini, E.; Dreassi, E.; Finetti, F.; Ievoli, G.; Macrì, G.; Petricci, E.; Rango, E.; Trabalzini, L.; Taddei, M. A pH-Responsive Crosslinker Platform for Antibody-Drug Conjugate (ADC) Targeting Delivery. *Chem. Commun.* **2022**, *58*, 10532–10535. [CrossRef]
11. Hao, Y.; Chen, Y.; He, X.; Yu, Y.; Han, R.; Li, Y.; Yang, C.; Hu, D.; Qian, Z. Polymeric Nanoparticles with ROS-Responsive Prodrug and Platinum Nanozyme for Enhanced Chemophotodynamic Therapy of Colon Cancer. *Adv. Sci.* **2020**, *7*, 2001853. [CrossRef]
12. Li, H.; Kim, H.; Xu, F.; Han, J.; Yao, Q.; Wang, J.; Pu, K.; Peng, X.; Yoon, J. Activity-Based NIR Fluorescent Probes Based on the Versatile Hemicyanine Scaffold: Design Strategy, Biomedical Applications, Outlook. *Chem. Soc. Rev.* **2022**, *51*, 1795–1835. [CrossRef]
13. He, Y.; Nie, Y.; Cheng, G.; Xie, L.; Shen, Y.; Gu, Z. Viral Mimicking Ternary Polyplexes: A Reduction-Controlled Hierarchical Unpacking Vector for Gene Delivery. *Adv. Mater.* **2014**, *26*, 1534–1540. [CrossRef]
14. Xu, X.; Zhou, X.; Xiao, B.; Xu, H.; Hu, D.; Qian, Y.; Hu, H.; Zhou, Z.; Liu, X.; Gao, J. Glutathione-Responsive Magnetic Nanoparticles for Highly Sensitive Diagnosis of Liver Metastases. *Nano Lett.* **2021**, *21*, 2199–2206. [CrossRef]

15. Kong, F.; Liang, Z.; Luan, D.; Liu, X.; Xu, K.; Tang, B. A Glutathione (GSH)-Responsive Near-Infrared (NIR) Theranostic Prodrug for Cancer Therapy and Imaging. *Anal. Chem.* **2016**, *88*, 6450–6456. [CrossRef]
16. He, S.; Li, J.; Lyu, Y.; Huang, J.; Pu, K. Near-Infrared Fluorescent Macromolecular Reporters for Real-Time Imaging and Urinalysis of Cancer Immunotherapy. *J. Am. Chem. Soc.* **2020**, *142*, 7075–7082. [CrossRef]
17. Jiang, M.; Wang, K.; Xiao, X.; Zong, Q.; Zheng, R.; Yuan, Y. Theranostic Heterodimeric Prodrug with Dual-Channel Fluorescence Turn-On and Dual-Prodrug Activation for Synergistic Cancer Therapy. *Adv. Healthc. Mater.* **2021**, *10*, 2101144. [CrossRef]
18. Yang, Z.; Fan, W.; Zou, J.; Tang, W.; Li, L.; He, L.; Shen, Z.; Wang, Z.; Jacobson, O.; Aronova, M.A. Precision Cancer Theranostic Platform by In Situ Polymerization in Perylene Diimide-Hybridized Hollow Mesoporous Organosilica Nanoparticles. *J. Am. Chem. Soc.* **2019**, *141*, 14687–14698. [CrossRef]
19. Lee, M.H.; Sharma, A.; Chang, M.J.; Lee, J.; Son, S.; Sessler, J.L.; Kang, C.; Kim, J.S. Fluorogenic Reaction-Based Prodrug Conjugates as Targeted Cancer Theranostics. *Chem. Soc. Rev.* **2018**, *47*, 28–52. [CrossRef]
20. Zhang, Y.-H.; Li, X.; Huang, L.; Kim, H.S.; An, J.; Lan, M.; Cao, Q.-Y.; Kim, J.S. AIE Based GSH Activatable Photosensitizer for Imaging-Guided Photodynamic Therapy. *Chem. Commun.* **2020**, *56*, 10317–10320. [CrossRef]
21. Wang, K.; Xiao, X.; Jiang, M.; Li, J.; Zhou, J.; Yuan, Y. An NIR-Fluorophore-Based Theranostic for Selective Initiation of Tumor Pyroptosis-Induced Immunotherapy. *Small* **2021**, *17*, 2102610. [CrossRef] [PubMed]
22. Zeng, X.; Li, X.; Sun, W. Highly Selective and Sensitive Colorimetric Chemosensor Based on Tricarboyanine for Detection of $Ag^{+}$ in Industrial Wastewater. *J. Leather Sci. Eng.* **2020**, *2*, 1–11. [CrossRef]
23. Li, X.-Q.; Wen, H.-Y.; Dong, H.-Q.; Xue, W.-M.; Pauletti, G.; Cai, X.-J.; Xia, E.W.-J.; Shi, D.; Li, Y.-Y. Self-Assembling Nanomicelles of A Novel Camptothecin Prodrug Engineered with A Redox-Responsive Release Mechanism. *Chem. Commun.* **2011**, *47*, 8647–8649. [CrossRef]
24. Wu, X.; Li, Y.; Lin, C.; Hu, X.-Y.; Wang, L. GSH- and pH-Responsive Drug Delivery System Constructed by Water-Soluble Pillar[5]arene and Lysine Derivative for Controllable Drug Release. *Chem. Commun.* **2015**, *51*, 6832–6835. [CrossRef] [PubMed]
25. Xie, F.; Su, P.; Pan, T.; Zhou, X.; Li, H.; Huang, H.; Wang, A.; Wang, F.; Huang, J.; Yan, H. Engineering Extracellular Vesicles Enriched with Palmitoylated ACE2 as COVID-19 Therapy. *Adv. Mater.* **2021**, *33*, 2103471. [CrossRef]
26. Li, X.; Kwon, N.; Guo, T.; Liu, Z.; Yoon, J. Innovative Strategies for Hypoxic-Tumor Photodynamic Therapy. *Angew. Chem. Int. Ed.* **2018**, *57*, 11522–11531. [CrossRef]